U.S. ARMY COMBAT CAPABILITIES DEVELOPMENT COMMAND
CHEMICAL BIOLOGICAL CENTER

ABERDEEN PROVING GROUND, MD 21010-5424

CCDC CBC-TR-1622

Reproducible 3D-Printed Unibody Drift Cells for Ion Mobility Spectrometry

Brian C. Hauck

SCIENCE AND TECHNOLOGY CORPORATION
Belcamp, MD 21017-1427

Patrick C. Riley
Bradley R. Ruprecht
Lester D. Strauch III

RESEARCH AND TECHNOLOGY DIRECTORATE

April 2020

Disclaimer

The findings in this report are not to be construed as an official Department of the Army position unless so designated by other authorizing documents.

REPORT DOCUMENTATION PAGE

Form Approved
OMB No. 0704-0188

1. REPORT DATE *(DD-MM-YYYY)*	**2. REPORT TYPE**	**3. DATES COVERED** *(From - To)*
XX-04-2020	Final	Feb 2019–Oct 2019

4. TITLE AND SUBTITLE
Reproducible 3D-Printed Unibody Drift Cells for Ion Mobility Spectrometry

5a. CONTRACT NUMBER

5b. GRANT NUMBER

5c. PROGRAM ELEMENT NUMBER

6. AUTHOR(S)
Hauck, Brian C. (STC); Riley, Patrick C.; Ruprecht, Bradley R.; and Strauch, Lester D. III (CCDC CBC)

5d. PROJECT NUMBER

5e. TASK NUMBER

5f. WORK UNIT NUMBER

7. PERFORMING ORGANIZATION NAME(S) AND ADDRESS(ES)
Science and Technology Corporation (STC); 111 C Bata Blvd., Belcamp, MD 21017-1427
Director, CCDC CBC, ATTN: FCDD-CBR-ID, APG, MD 21010-5424

8. PERFORMING ORGANIZATION REPORT NUMBER
CCDC CBC-TR-1622

9. SPONSORING / MONITORING AGENCY NAME(S) AND ADDRESS(ES)
U.S. Army Combat Capabilities Development Command Chemical Biological Center, Aberdeen Proving Ground, MD 21010-5424

10. SPONSOR/MONITOR'S ACRONYM(S)
CCDC CBC

11. SPONSOR/MONITOR'S REPORT NUMBER(S)

12. DISTRIBUTION / AVAILABILITY STATEMENT
Approved for public release: distribution unlimited.

13. SUPPLEMENTARY NOTES
U.S. Army Combat Capabilities Development Command Chemical Biological Center (CCDC CBC) was previously known as U.S. Army Edgewood Chemical Biological Center (ECBC).

14. ABSTRACT: (Limit 200 words)
Ion mobility spectrometry-based detectors exhibit a range of reduced ion mobility (K_0) values when exposed to the same chemical under identical conditions. One component of instrument accuracy that may contribute to this variation is the manufacturing process of mass-produced systems. Mass-produced ion mobility drift cells often consist of individual electrodes separated only by air, and their position and angle may vary between units due to human error during construction. These errors will create inhomogeneous electric fields and differing physical lengths among drift cells. The ultimate effect will be a discrepancy between the true ion path length and the intended drift length of the drift cell. It is hypothesized that this ultimately contributes to observed differences in peak shape and position and the resulting range of K_0 values seen for identical detectors. Here, we report on a unibody ion mobility drift cell that is constructed using 3D printing and consists of fused and alternating conductive and insulating layers of preprogrammed and reproducible length. The reproducibility in the length across multiple drift cell prints was assessed using 2,6-di-*tert*-butylpyridine as an accurate ion mobility calibrant.

15. SUBJECT TERMS

3D printing	Unibody drift cell	Accuracy
Additive manufacturing	Ion mobility spectrometry (IMS)	Precision

16. SECURITY CLASSIFICATION OF:			**17. LIMITATION OF ABSTRACT**	**18. NUMBER OF PAGES**	**19a. NAME OF RESPONSIBLE PERSON**
a. REPORT	**b. ABSTRACT**	**c. THIS PAGE**			Renu B. Rastogi
U	U	U	UU	26	**19b. TELEPHONE NUMBER** *(include area code)* (410) 436-7545

Standard Form 298 (Rev. 8-98)
Prescribed by ANSI Std. Z39.18

Blank

PREFACE

The work described in this report was authorized under the Innovative Development of Employee Advanced Solutions (IDEAS) program of the U.S. Army Combat Capabilities Development Command Chemical Biological Center (CCDC CBC; Aberdeen Proving Ground, MD), as a part of FY19 § 2363 funds. The work was started in February 2019 and completed in October 2019.

The use of either trade or manufacturers' names in this report does not constitute an official endorsement of any commercial products. This report may not be cited for purposes of advertisement.

This report has been approved for public release.

Acknowledgments

The authors acknowledge Dr. Augustus Way Fountain (CCDC CBC, retired) and Mr. Adam Seiple (CCDC CBC) for their support of this program.

Blank

CONTENTS

FIGURES

TABLES

REPRODUCIBLE 3D-PRINTED UNIBODY DRIFT CELLS FOR ION MOBILITY SPECTROMETRY

1. INTRODUCTION

Ion mobility spectrometry (IMS) is a widely used analytical technique for the separation and identification of ions based on their size-to-charge ratios (Ω/z). An IMS drift tube consists of a series of electrodes to which a voltage (V) gradient is applied and a weak electric field is established. An ionization source creates background reactant ions that react with chemical vapors to produce product ions in the reaction region of the drift tube. This mixture of reactant and product ions is pulsed into a drift region (cell) of known length (L), where they drift under the electric field toward a detector (often a grounded Faraday plate [FP]) when the drift tube is not used in tandem with other instrumentation such as mass spectrometry. Larger ions collide more often with the molecules of a counter-current neutral drift gas, reducing their terminal velocity and separating them from smaller ions. Upon neutralization on the FP, the drift time (t_d) of each ion across L is recorded. Ions are identified by their reduced ion mobility (K_0) values, which are calculated using eq 1 with the temperature (T) and pressure (P) of the drift gas being standardized against standard temperature and pressure.[1] It is important to note that V, t_d, T, and P must be directly correlated to L to accurately calculate the K_0 values of ions.[2,3]

$$K_0 = \frac{L^2}{V t_d}\left(\frac{273.15}{T}\right)\left(\frac{P}{760}\right) \quad (1)$$

IMS has a widespread application to multiple fields including national security,[4,5] drug detection[6] and screening,[7] pharmaceutical[8] and biomedical studies,[9] and environmental[10] and food sciences.[11] IMS-based devices are well established within the commercial space, and more than 60,000 detectors are produced and deployed in national security settings alone.[12] It is critical that these IMS-based detectors are constructed in such a manner so as to be consistent across devices. Many models of drift cells are hand-assembled: electrodes are attached to a printed circuit board with only air separating them, to isolate their applied voltages. However, this may introduce human error and variability in L between drift cells, due to slight variations in the placement or angle of individual electrodes. If the placement of the ion gate or FP varies between units along the axis of ion drift, the true length of the drift cell will deviate from the L as designed. Any electrodes that are not concentric or parallel to the rest will alter the path of ion drift and deviate the true path length from the L as designed. It is theorized that this may contribute to the differences in responses from multiple devices exposed to the same chemical under identical conditions.[4] In a unibody drift cell, an electrically insulating material is fused between each electrode, thereby eliminating the possibility of variable electrode positions. Traditional laboratory-grade drift tubes are often made of stacked rings of stainless steel electrodes and alumina insulators. However, earlier techniques for unibody drift cell construction, such as metal-to-ceramic brazing, cementing, or resistive glass formulations, are expensive and time consuming. Additionally, these techniques yield structurally fragile final products that are not suitable for incorporation into rugged and mass-produced devices.[2,3,13–15]

Additive manufacturing, also known as 3D printing, offers an inexpensive solution to achieving a unibody drift cell of known and reproducible L. Fused deposition modeling is an extrusion-based 3D-printing technique in which molten material is selectively deposited from a heated extruder nozzle, layer by layer, to create a final object that is based on a computer-aided design (CAD) model.[16] Hollerbach et al. have previously 3D-printed individual conductive electrodes for use in an IMS drift tube.[17,18] However, these 3D-printed electrodes were still hand-assembled into a stacked ring configuration and held in place by an insulating clamshell housing. Here, we report on the use of 3D printing to construct unibody IMS drift cells of fused and alternating electrode and insulation layers. We have assessed the reliability of the method to reproduce a preprogrammed L in multiple drift cells by measuring the t_d of 2,6-di-*tert*-butylpyridine (D*t*BP) between two ion gates on either end of the 3D-printed unibody drift cell and then back-calculating L in eq 1, based on the accurate K_0 value of 1.477 ± 0.001 $cm^2V^{-1}s^{-1}$ for $(DtBP)H^+$.[19]

2. MATERIAL AND METHOD

2.1 3D-Printing Parameters

A LulzBot Taz 5 3D printer with a Dual Extruder v3 tool head (Aleph Objects, Inc.; Loveland, CO) was used to print the reaction region and a transition region into a mass spectrometer. A BCN3D Sigma R19 (BCN3D Technologies; Barcelona, Spain) 3D printer was used to print the interchangeable drift cells and an insulating sleeve because a persistent clogging issue occurred with use of the LulzBot Taz 5 dual extruder tool head. Two forms of polyethylene terephthalate glycol (PETG) filament (3DXTech; Grand Rapids, MI) were used to 3D print the unibody IMS drift tube components. 3DXSTAT electrostatic discharge (ESD)-Safe PETG doped with carbon nanotubes was used to create the conductive electrode layers, and natural-colored MAX-G PETG was used to create nonconductive insulator layers. At low extruder temperatures, the ESD-Safe PETG remains nonconductive, but the ESD-Safe property fails, and the filament becomes conductive when extruded at high temperatures.[17,18] Polyacetic acid (PLA) and acrylonitrile butadiene styrene (ABS) were also tested as insulating materials. PLA consistently clogged the LulzBot Taz 5 3D printer, and ABS did not bond well to the ESD-Safe PETG.

Characteristics of both printers included a 0.8 mm vertical retraction lift, a 0.2 mm primary layer height, and a 99% infill percentage. The extruder temperatures were 275 °C for the conductive ESD-Safe PETG and 245 °C for the nonconductive PETG. The ESD-Safe PETG can also be used for the nonconductive layers if they are extruded at 205 °C on the LulzBot Taz 5 3D printer. This, however, was not extensively investigated on the BCN3D Sigma R19 3D printer. Support was not generated for parts, and no adhesion material was used for the printing bed. All extruders used a 15 mm prime pillar, a single layer and single outline skirt offset by 4 mm from the parts, and a single outline ooze shield offset by 2 mm from the parts. Remaining settings that differed between the two printers are shown in Table 1.

Table 1. LulzBot Taz 5 and BCN3D Sigma R19 Printing Parameters

Printing Parameter (unit)	LulzBot Taz 5	BCN3D Sigma R19
Nozzle diameter (mm)	0.5	0.4
Extrusion multiplier	0.9	1
Retraction (mm)	5.0	5.8
Retraction speed (mm/min)	1,800	4,000
Coasting distance (mm)	Off	0.2
Bed temperature (°C)	70	90
Printing speed (mm/min)	3,600	3,000

2.2 General Design

All components of the IMS drift tube were printed along the axis of ion drift from the end farthest from the ionization source to the end closest to the ionization source. The assembly of the IMS drift tube is depicted in Figure 1. The inner diameter was 5 cm, and the outer diameter was 6 cm. The electrode layers (black) were 1 cm long, and the insulating layers (white) were 0.6 cm long. The drift tube was divided into six components: a preexisting corona ionization source (gray),[19] a unibody reaction region, two Bradbury–Nielson (BN) ion gates (beige) on either end of the unibody drift cell, and a unibody transition region into a time-of-flight mass spectrometer (TOFMS).

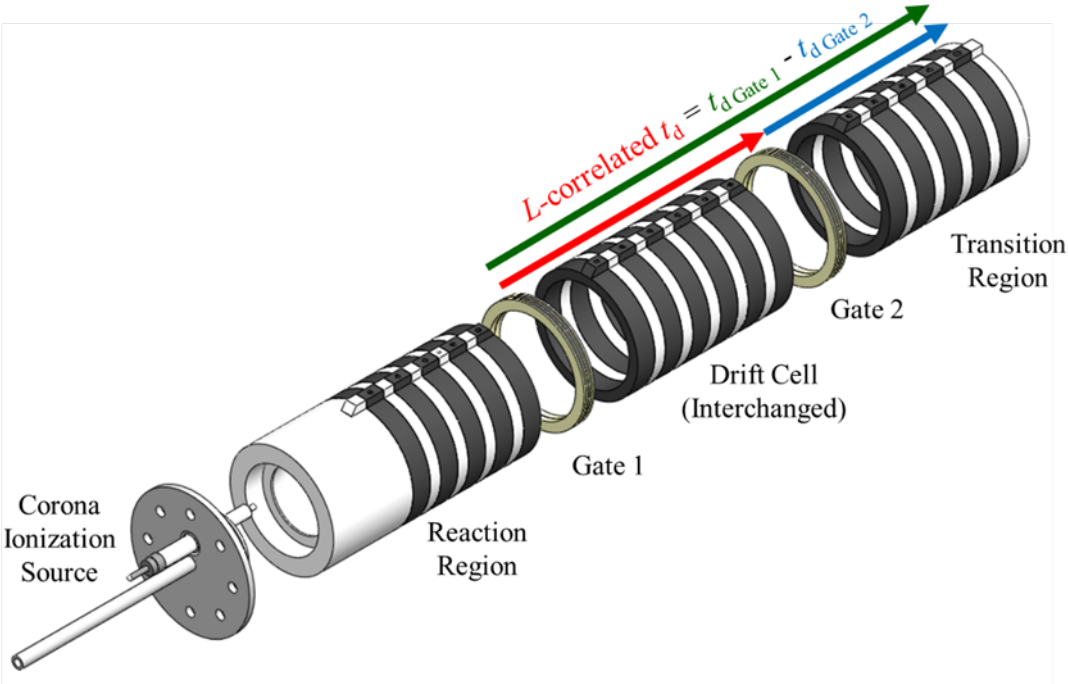

Figure 1. CAD model depicting an exploded view of the six IMS drift tube components.

The top of each 3D-printed unibody component featured a 0.6 cm wide by 0.4 cm high ridge with a 1.78 mm o.d. by 0.7 cm deep hole in each electrode layer. The holes were hand-tapped, and 4 in. long, 2-56 threaded rods were screwed into the holes to supply high voltage to the electrode layers. The threaded holes on either side of the BN ion gates passed through to the drift space and allowed for the insertion of T100-250 temperature probes coupled to an F200 precision thermometer (Isotech; Colchester, VT) after the threaded rods were removed. A 4.25 mm long, 35° chamfer at the end of the ridges on either side of the BN ion gates allowed sufficient room for the electrical leads of the gates. The IMS drift tube components were loaded in series, as shown in Figure 1, into a 3D-printed insulating sleeve and a preexisting grounded thermal case.

2.2.1 Unibody Reaction Region

The reaction region consisted of a 4.6 cm long insulating layer followed by five electrode layers and four insulating layers. The total length of the reaction region was 12 cm, and it required 9 h to print. The printing process of the reaction region was paused after completing the electrode layer closest to the ionization source, and a 20 × 20 mesh, stainless steel wire cloth disk (McMaster-Carr; Elmhurst, IL) was embedded into a printed seat in its front face to act as the corona ionization counter electrode. Printing of the remaining 4.6 cm long insulating layer was resumed. Its inner diameter featured a 3.5 cm long, 16.9° chamfer to meet the base of the corona ionization source.

2.2.2 Unibody Drift Cells

Ten reproducible unibody drift cells were printed. One was printed individually (designated Group 0), and the remaining nine were printed in three groups of three cells (designated Groups 1–3) to determine variability within a single printing group as well as between printing groups. The single drift cell required 10 h to print, and a group of three took 24 h. The drift cells featured six electrode layers and five insulating layers for a total printed length of 9 cm.

2.2.3 BN Ion Gates

The BN ion gates were made of 0.3 cm long alumina halves cemented together using Resbond 920 ceramic adhesive (Cotronics Corp.; Brooklyn, NY) with two interleaved sets of parallel and electrically isolated 0.003 in. o.d. Alloy 46 wires (California Fine Wire Company; Grover Beach, CA) spaced on 0.005 in. centers. The BN ion gates were made in this traditional manner because multiple attempts to incorporate the wires into the 3D-printing process had failed. When the parallel set of wires was placed on a printed portion of the drift tube, the filament failed to adhere to them as it attempted to print the remaining portion of the drift tube.

2.2.4 Unibody Transition Region

The transition region before the TOFMS interface featured five alternating electrode and insulator layers for a total length of 8 cm and a print time of 6 h. The last insulating layer separated the last electrode layer from the grounded TOFMS interface housing. The last electrode layer featured a 3.3 mm o.d. hole to insert 1/8 in. o.d. stainless steel tubing for introduction of the drift gas.

2.3 Instrumental Parameters

2.3.1 IMS Drift Tube

A drift L of 9.6 cm was initially calculated based on the 9 cm programmed length and two 0.3 cm gate halves on either end of the drift cell. Each BN ion gate was installed in the same location and orientation, so as not to introduce such variability in L between drift cell prints. Each unibody drift cell was interchanged between the two BN ion gates to collect ion mass mobility spectra. A first spectrum was collected by operating Gate 1 with a 200 µs gate pulse width, while Gate 2 was connected to the high-voltage gradient to maintain a uniform electric field. Electrical leads between the BN ion gates were then switched, and a second spectrum from Gate 2 was collected. Spectra were collected in triplicate from each BN ion gate.

An electric field of 277.9 ± 0.1 V/cm was established by an LS020 reversible 20 kV power supply (Applied Kilovolts Ltd; West Springfield, MA) and a series of 20 MΩ resistors (±1%; Caddock Electronics, Inc.; Riverside, CA). The BN ion gate reference lead was created between two 10 MΩ resistors. A 1 MΩ resistor (±1%, Caddock Electronics) and a 5 MΩ variable resistor (Newark Electronics; Chicago, IL) adjusted the remaining resistance before ground, to maintain a uniform electric field into the TOFMS. Each resistor and the high voltages applied to the first electrode layer and gate references were directly measured with an 8846A digital multimeter (Fluke Corp.; Everett, WA) and a 250-G-10 high-voltage probe (CPS High Voltage; Tigard, OR). Direct voltage measurements were corrected to compensate for current drawdown through the high-voltage probe.[2] The preexisting corona ionization source consisted of a 20 kV high-voltage feedthrough (Solid Sealing Technology; Watervliet, NY) welded above the central drift gas exit of an Alloy 46 base. Voltage was supplied to the feedthrough by a molded silicone high-voltage plug (Solid Sealing Technology), and a corona was established by a 50 µm diameter stainless steel wire (McMaster-Carr) wrapped around the opposite end of the feedthrough. The corona ionization source was held at a 2.3 kV bias above the counter electrode by a second LS020 reversible 20 kV power supply.

The drift tube was held at room temperature, and the directly measured drift gas temperature between the front of the first gate and the back of the second gate was 24.82 ± 0.04 °C. Ambient P in the laboratory was measured by a Princo model 453 standard mercurial barometer (Precision Thermometer & Instrument Co.; Philadelphia, PA), and measurements were corrected for temperature and latitude. L was back-calculated in triplicate for each unibody drift cell using eq 1, in which the K_0 value of $(D\textit{t}BP)H^+$ was 1.477 $cm^2V^{-1}s^{-1}$, V was the difference in voltage measurements between each BN ion gate reference lead, t_d was the difference in the measured protonated monomer ion of D*t*BP $[(D\textit{t}BP)H^+]$ t_d from each gate, T was the average drift gas temperature, and P was the pressure measured after saving each Gate 1 spectrum. In this way, V, t_d, T, and P were all directly correlated to the L of each unibody drift cell.

2.3.2 TOFMS

As shown in Figure 1, the six components of the IMS drift tube were stacked inside a 3D-printed insulating sleeve, which was in turn inserted into a preexisting aluminum thermal case. The thermal case containing the IMS drift tube was interfaced to a TOFMS (Ionwerks, Inc.; Houston, TX) to mass-identify ion drift time peaks. A plate was screwed onto

the front of the thermal case, which partially compressed a set of four screws between the front plate and the ionization source, to hold the drift tube components in place. For all interchanged drift cells, screws were tightened to the same degree so as not to compress the 3D-printed parts or vary the force applied to hold each drift cell in place and thereby introduce variability into *L*.

The TOFMS vacuum interface had a 300 μm pinhole, and ions were orthogonally extracted into a V-shaped flight path before being detected by microchannel plates (Photonis; Sturbridge, MA) in a chevron stack orientation. SH-110 and TriScroll 600 dry scroll pumps and V 75 and V 250 turbo pumps (Agilent Technologies, Inc.; Santa Clara, CA) established pressures of 1.8 Torr in the vacuum interface, 7.0×10^{-2} Torr in the ion focusing region, and 3.0×10^{-6} Torr in the flight region. Ion mass mobility spectra were generated and analyzed by software developed at Ionwerks and run on the IDL Virtual Machine platform (L3Harris Geospatial Solutions; Broomfield, CO).

2.4 Chemicals

D*t*BP was obtained from Sigma-Aldrich Chemical Co. (St. Louis, MO) as a 97% pure standard. A wash bottle (VWR International; Radnor, PA) was saturated with D*t*BP vapor and used as needed to flush sample vapor through an EZRU21 external/internal reducing union (Valco Instruments Co., Inc.; Houston, TX) and a silica capillary (150 μm i.d., 360 μm o.d.; Polymicro Technologies; Phoenix, AZ) inserted into a 1.6 mm o.d. hole printed in the third insulating layer of the reaction region. A 1.00 ± 0.01 L/min flow of compressed house-air drift gas was supplied by an 1179A digital mass flow controller and 247D power supply and readout (MKS Instruments; Andover, MA). A LabVIEW program (National Instruments; Austin, TX) recorded the water content of the drift gas from a Moisture Image Series 1 hygrometer and probe (GE Measurement and Control; Fairfield, CT), and the average water content for all collected spectra was 0.5 ± 0.1 ppmv. A certified Trace Source disposable ammonia permeation tube (Kin-Tek; La Marque, TX) was inserted in-line with the drift gas after the hygrometer probe to create a 20 ppmv drift gas dopant. Doing so eliminated the $H(H_2O)_n^+$ reactant ion peak in favor of an $H(NH_3)_n^+$ reactant ion peak, and ammonia dopant was present in both the drift and reaction regions of the IMS drift tube.

3. RESULTS AND DISCUSSION

3.1 Electrode Conductivity and Isolation

The temperature at which to extrude the electrode layers was determined by printing a series of separate ESD-Safe PETG electrode rings in 5 °C intervals between 265 and 290 °C. A voltage of 3000.75 ± 0.01 V was applied to one end of each ring and then measured on the opposite end to determine any loss in voltage. The results in Figure 2 show that the conductivity across the ring increased as a function of temperature until 275 °C, when resistance was minimal and matched the applied voltage. It was observed that the ESD-Safe PETG tended to degrade at extruder temperatures in excess of 275 °C.

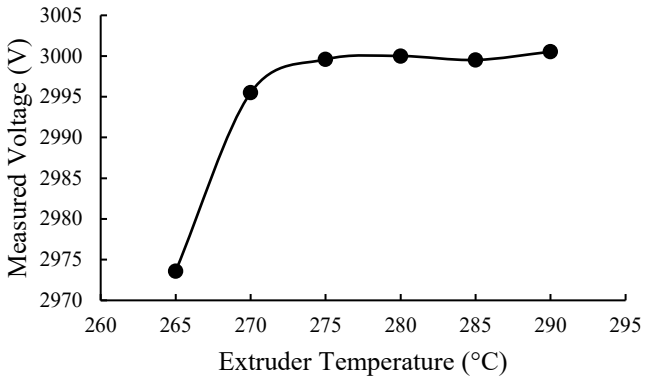

Figure 2. Conductivity of 3D-printed electrode layers as a function of extruder temperature.

Electrical isolation of electrode layers was tested by printing a unibody section of five electrode layers and six insulator layers on the LulzBot Taz 5 system, as outlined in Table 1. A voltage gradient was established by attaching each electrode layer to a series of 20 MΩ resistors and applying 3000.02 ± 0.02 V to the first electrode layer. The voltage of each subsequent electrode layer was directly measured and compared to its expected voltage (as calculated by Ohm's law) from the first electrode layer voltage, as shown in Table 2. All electrodes had less than a 0.1% difference from the expected voltage, which indicates that the MAX-G PETG sufficiently created electrical isolation between each ESD-Safe PETG electrode to establish an electric field. The voltage gradient failed only when electrode layers were arbitrarily bridged by a conductor.

Table 2. Isolation between Electrodes and Establishment of a Voltage Gradient

Electrode Number	Measured Voltage (V)	% Difference from Expected Voltage
1	3,000.02 ± 0.02	*
2	2,400.34 ± 0.04	0.01
3	1,801.72 ± 0.02	0.08
4	1,200.95 ± 0.02	0.06
5	600.51 ± 0.02	0.09

*3 kV was applied to electrode number 1 and was used to calculate the expected voltage of all subsequent electrodes.

3.2 Physically Measured Length and Mass

The printed length and mass of each unibody drift cell were measured, as shown in Table 3, to assess the uniformity of prints across and within groups. Drift cells of the same number in different groups were printed in the same position on the printer bed. Each measurement in Table 3 is an average of four individual measurements.

Table 3. Physically Measured Mass and Length of Each 3D-Printed Unibody Drift Cell

Group Number	Drift Cell Number	Mass (g)	Physically Measured *L* (cm)
0	1	98.0850 ± 0.0001	9.020 ± 0.005
1	1	97.8932 ± 0.0001	9.027 ± 0.005
	2	98.6186 ± 0.0002	9.038 ± 0.005
	3	98.2505 ± 0.0003	9.029 ± 0.004
2	1	97.7504 ± 0.0004	9.016 ± 0.004
	2	98.349 ± 0.001	9.031 ± 0.005
	3	98.1753 ± 0.0005	9.022 ± 0.003
3	1	97.9130 ± 0.0003	9.024 ± 0.005
	2	98.4946 ± 0.0002	9.042 ± 0.004
	3	98.3333 ± 0.0002	9.034 ± 0.003
Overall average		98.2 ± 0.3	9.03 ± 0.01

The average mass of all unibody drift cells was 98.2 ± 0.3 g, representing a 0.3% variability in the amount of filament used in each drift cell. The overall average length was 9.03 ± 0.01 cm, which represents a 0.1% variability and a 0.3% difference from the programmed length of 9 cm. This indicates that 3D printing is a viable method for reproducing a programmed length for IMS components. There does not appear to be any significant pattern or difference in the measured mass or *L* within or between printed groups. The consistency and performance of the prints was further tested by loading them into the IMS drift tube and back-calculating their lengths between the two BN ion gates.

3.3 Back-Calculated Drift Length

When the IMS drift cells were installed in the drift tube, the background produced by the corona ionization source showed mass-to-charge ratio (*m/z)* 18 and 35 reactant ions, corresponding to $H(NH_3)_n^+$, and various *m/z* peaks indicating that volatile organic chemicals (VOCs) were off-gassing from the unibody drift cell, as shown in Figure 3a. However, when D*t*BP was introduced, the VOCs were eliminated, and $(DtBP)H^+$ was the only product ion at *m/z* 192 before returning to the background spectrum. The unibody drift cells were not put through any thermal bake-out procedure so as not to risk altering the shape or dimensions of the drift cells. D*t*BP was chosen as the mobility standard because its protonated amine is sufficiently protected by steric hindrance to prevent VOCs and other neutrals from clustering with it and altering its K_0 value.[19,20]

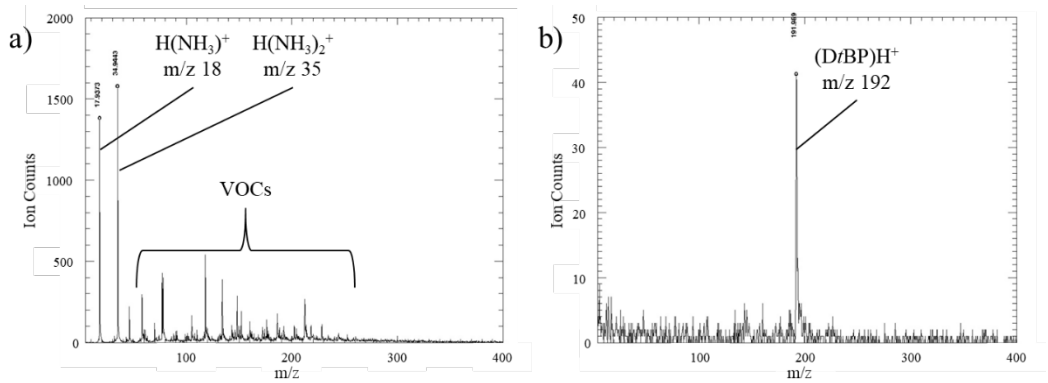

Figure 3. (a) Corona ionization background of the unibody drift cells; and (b) sole product ion peak when D*t*BP was introduced into the reaction region.

Table 4 shows the results of back-calculating the L of each 3D-printed unibody drift cell based on the accurate $(D tBP)H^+$ K_0 value of 1.477 ± 0.001 $cm^2V^{-1}s^{-1}$. The back-calculated L of each unibody drift cell is an average of three t_d-corrected spectra, and the average L across all unibody drift cells was 9.68 ± 0.01 cm, which represents 0.1% variability. The additional 0.68 cm to the programmed 9 cm L accounts for the 0.6 cm that was contributed by the two 0.3 cm gate halves on either end of the drift region and 800 µm contributed by the thickness of the ceramic adhesive and gate wires in both BN ion gates. The average back-calculated L of 9.68 cm was then used to calculate the K_0 value of $(D tBP)H^+$ for all t_d-corrected spectra collected. The average calculated K_0 value across all t_d-corrected spectra, based on this true calibrated L, was 1.476 ± 0.003 $cm^2V^{-1}s^{-1}$. This represents a 0.2% variability, which is still an order of magnitude improvement over other IMS-based systems and a 0.1% difference from the accurate K_0 value of $(D tBP)H^+$.[4,19] There does not appear to be any significant pattern or difference in the back-calculated L within or between the printed groups.

Table 4. Back-Calculated L between Two BN Ion Gates and K_0 Values Calculated from the Average L for Each Unibody Drift Cell

Group Number	**Drift Cell Number**	**Back-Calculated *L* (cm)**	**K_0 Value Calculated from Average *L* ($cm^2V^{-1}s^{-1}$)**
0	1	9.68 ± 0.01	1.478 ± 0.002
1	1	9.686 ± 0.001	1.4753 ± 0.0003
	2	9.68 ± 0.01	1.478 ± 0.002
	3	9.67 ± 0.01	1.479 ± 0.002
2	1	9.687 ± 0.003	1.475 ± 0.001
	2	9.69 ± 0.01	1.474 ± 0.002
	3	9.67 ± 0.01	1.481 ± 0.002
3	1	9.679 ± 0.004	1.477 ± 0.001
	2	9.695 ± 0.005	1.473 ± 0.001
	3	9.702 ± 0.003	1.470 ± 0.001
Overall average		9.68 ± 0.01	1.476 ± 0.003

3.4 Frequency of Occurrence Analysis

As shown in Figure 4, frequency of occurrence analyses for (D*t*BP)H^+ K_0 values were performed for the 30 spectra produced by the 10 3D-printed unibody drift cells and for a random selection of 62 D*t*BP spectra from four handheld IMS-based devices of identical design that featured traditional air-insulated electrodes. The four handheld IMS-based devices exhibited a bimodal distribution (orange trace) of the reported K_0 values for (D*t*BP)H^+, whereas the K_0 values from the 10 3D-printed unibody drift cells were more Gaussian in their distribution (blue trace). This indicates improved reproducibility in the performance of the 3D-printing construction method.

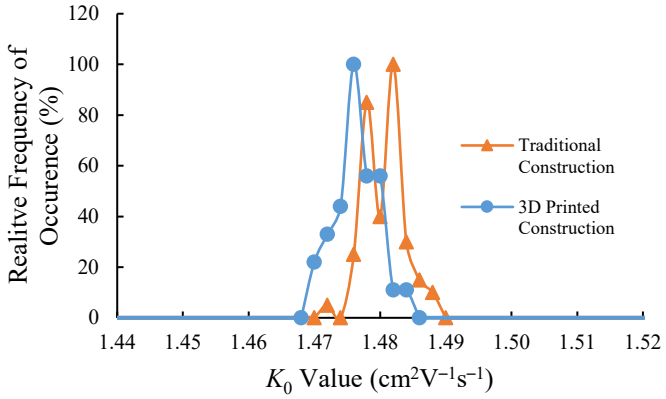

Figure 4. Frequency of occurrence analyses for 10 3D-printed unibody drift cells (blue circles) and four handheld IMS-based devices with traditionally constructed drift cells (orange triangles).

4. CONCLUSIONS

We have shown the first use of 3D printing to construct a unibody IMS drift cell consisting of fused alternating layers of electrically conductive and insulating PETG polymer. The electrode layers were sufficiently conductive, while the insulating layers were sufficiently nonconductive, so as to establish the voltage gradient and electric field. 3D printing is a viable method to reliably reproduce IMS drift cells of known length. These unibody drift cells were reproducible to within 0.3% of the programmed length and 0.1% of other drift cells when L was both physically measured and accurately calibrated using D*t*BP. This reproducible L maintained an accuracy of 0.1% and a precision of 0.2% in the calculated K_0 value of (D*t*BP)H^+. This represents an order of magnitude improvement in performance over earlier, comparatively inaccurate IMS-based devices.

The filament materials used in the 3D printing released VOCs that were ionized by corona ionization. A method for baking out the 3D-printed part and eliminating these VOCs must be developed if the unibody drift cell is to be used in IMS-based devices. Otherwise, the risk exists that the drift tube will not be able to ionize chemicals of interest, or their ion mobility peaks will be lost in convoluted spectra. The bake-out procedure also must not alter the dimensions of the drift cell, to avoid negating the benefit of reproducible 3D printing. Therefore,

other polymer materials may be more suitable than ESD-Safe PETG and PETG; determining this would require an exploration of off-gassing and bonding properties. However, the current design and materials are durable, affordable, and well suited for mass producing throwable or disposable technologies.

Currently, only the drift region has been continuously 3D printed. An ion gate, aperture grid, and FP need to be incorporated into the design to make an entirely unibody IMS instrument. The 3D-printed unibody drift cell dimensions also need to be minimized from the current laboratory-grade size, while the number of electrodes is maximized. This will decrease the time required to print the parts as well as facilitate the integration of swappable component-based parts into portable and handheld commercial IMS-based devices.

Blank

LITERATURE CITED

1. Eiceman, G.A.; Karpas, Z.; Hill, H.H., Jr. *Ion Mobility Spectrometry*, 3rd ed.; CRC Press: Boca Raton, FL, 2014.

2. Hauck, B.C.; Siems, W.F.; Harden, C.S.; McHugh, V.M.; Hill, H.H., Jr. *E/N* Effects on K_0 Values Revealed by High Precision Measurements under Low Field Conditions. *Rev. Sci. Instrum.* **2016,** *87,* 075104.

3. Hauck, B.C.; Siems, W.F.; Harden, C.S.; McHugh, V.M.; Hill, H.H., Jr. Construction and Evaluation of a Hermetically Sealed Accurate Ion Mobility Instrument. *Int. J. Ion Mobil. Spec.* **2017,** *20* (3–4), 57–66.

4. Hauck, B.C.; Harden, C.S.; McHugh, V.M. Current Status and Need for Standards in Ion Mobility Spectrometry. *Int. J. Ion Mobil. Spec.* **2018,** *21,* 105–123.

5. Ewing, R.G.; Atkinson, D.A.; Eiceman, G.A.; Ewing, G.J. A Critical Review of Ion Mobility Spectrometry for the Detection of Explosives and Explosive Related Compounds. *Talanta* **2001,** *54,* 515–529.

6. Forbes, T.P.; Lawrence, J.; Verkouteren, J.R.; Verkouteren, R.M. Discriminative Potential of Ion Mobility Spectrometry for the Detection of Fentanyl and Fentanyl Analogues Relative to Confounding Environmental Interferents. *Analyst* **2019,** *144,* 6391–6403.

7. Lu, Y.; O'Donnell, R.M.; Harrington, P.B. Detection of Cocaine and Its Metabolites in Urine Using Solid Phase Extraction-ion Mobility Spectrometry with Alternating Least Squares. *Forensic Sci. Int.* **2009,** *189,* 54–59.

8. Weston, D.J.; Bateman, R.; Wilson, I.D.; Wood, T.R.; Creaser, C.S. Direct Analysis of Pharmaceutical Drug Formulations Using Ion Mobility Spectrometry/Quadrupole-Time-of-Flight Mass Spectrometry Combined with Desorption Electrospray Ionization. *Anal. Chem.* **2005,** *77,* 7572–7580.

9. Zhang, X.; Quinn, K.; Cruickshank-Quinn, C.; Reisdorph, R.; Reisdorph, N. The Application of Ion Mobility Mass Spectrometry to Metabolomics. *Curr. Opin. Chem. Biol.* **2018,** *42,* 60–66.

10. Zheng, X.; Dupuis, K.T.; Aly, N.A.; Zhou, Y.; Smith, F.B.; Tang, K.; Smith, R.D.; Baker, E.S. Utilizing Ion Mobility Spectrometry and Mass Spectrometry for the Analysis of Polycyclic Aromatic Hydrocarbons, Polychlorinated Biphenyls, Polybrominated Diphenyl Ethers and Their Metabolites. *Anal. Chim. Acta* **2018,** *1037,* 265–273.

11. Gerhardt, N.; Birkenmeier, M.; Schwolow, S.; Rohn, S.; Weller, P. Volatile-Compound Fingerprinting by Headspace-Gas-Chromatography Ion -Mobility Spectrometry (HS-GC-IMS) as a Benchtop Alternative to ^{1}H NMR Profiling for Assessment of the Authenticity of Honey. *Anal. Chem.* **2018,** *90* (3), 1777–1785.

12. Eiceman, G.A.; Stone, J.A. Ion Mobility Spectrometers in National Defense. *Anal. Chem.* **2004,** *76* (21), 390A–397A.

13. Kaplan, K.; Graf, S.; Tanner, C.; Gonin, M.; Fuhrer, K.; Knochenmuss, R.; Dwivedi, P.; Hill, H.H., Jr. Resistive Glass IM-TOFMS. *Anal. Chem.* **2010,** *82* (22)*,* 9336–9343.

14. Kwasnik, M.; Fuhrer, K.; Gonin, M.; Barbeau, K.; Fernández, F.M. Performance, Resolving Power, and Radial Ion Distributions of a Prototype Nanoelectrospray Ionization Resistive Glass Atmospheric Pressure Ion Mobility Spectrometer. *Anal. Chem.* **2007,** *79* (20)*,* 7782–7791.

15. Kwasnik, M.; Fernández, F.M. Theoretical and Experimental Study of the Achievable Separation Power in Resistive-Glass Atmospheric Pressure Ion Mobility Spectrometry. *Rapid Commun. Mass Spectrom.* **2010,** *24,* 1911–1918.

16. Ligon, S.C.; Liska, R.; Stampfl, J.; Gurr, M.; Mülhaupt, R. Polymers for 3D Printing and Customized Additive Manufacturing. *Chem. Rev.* **2017,** *117* (15)*,* 10212–10290.

17. Hollerbach, A.; Baird, Z.; Cooks, R.G. Ion Separation in Air Using a Three-Dimensional Printed Ion Mobility Spectrometer. *Anal. Chem.* **2017,** *89* (9), 5058–5065.

18. Hollerbach, A.; Fedick, P.W.; Cooks, R.G. Ion Mobility–Mass Spectrometry Using a Dual-Gated 3D Printed Ion Mobility Spectrometer. *Anal. Chem.* **2018,** *90* (22), 13265–13272.

19. Hauck, B.C.; Harden, C.S.; McHugh, V.M. Accurate Evaluation of Potential Calibration Standards for Ion Mobility Spectrometry. *Anal. Chem.* **2020**, *92* (8), 6158–6165.

20. Valadbeigi, Y.; Ilbeigi, V.; Michalczuk, B.; Sabo, M.; Matejcik, S. Study of Atmospheric Pressure Chemical Ionization Mechanism in Corona Discharge Ion Source with and without NH_3 Dopant by Ion Mobility Spectrometry Combined with Mass Spectrometry: A Theoretical and Experimental Study. *J. Phys. Chem. A* **2019,** *123,* 313–322.

ACRONYMS AND ABBREVIATIONS

Ω/z	ion size-to-charge ratio
ABS	acrylonitrile butadiene styrene
AM	additive manufacturing
BN	Bradbury–Nielson
CAD	computer-aided design
D*t*BP	2,6-di-*tert*-butylpyridine
$(D\textit{t}BP)H^+$	protonated monomer ion of D*t*BP
ESD	electrostatic discharge
FDM	fused deposition modeling
FP	Faraday plate
IMS	ion mobility spectrometry
K_0	ion mobility value
L	ion drift length
m/z	mass-to-charge ratio
P	drift gas pressure
PETG	polyethylene terephthalate glycol
PLA	polyacetic acid
T	drift gas temperature
t_d	ion drift time
TOFMS	time-of-flight mass spectrometer
V	drift voltage gradient
VOC	volatile organic compound

DISTRIBUTION LIST

The following individuals and organizations were provided with one Adobe portable document format (pdf) electronic version of this report:

U.S. Army Combat Capabilities Development Command Chemical Biological Center (CCDC CBC)
FCDD-CBR-ID
ATTN: Hauck, B.
Riley, P.
Harden, C.
McHugh, V.
Wade, M.
Ruprecht, B.
Strauch, L.
Wallace, K.

Joint Project Manager for Chemical, Biological, Radiological and Nuclear Sensors
ATTN: Matz, C.
Powers, M.
Weible, M.

Defense Threat Reduction Agency Joint Science and Technology Office
ATTN: Cleary, C.
Quinn, K.
James, A.
O'Connor, K.
Minyard, M.

CCDC CBC Technical Library
FCDD-CBR-L
ATTN: Foppiano, S.
Stein, J.

Defense Technical Information Center
ATTN: DTIC OA

U.S. ARMY COMBAT CAPABILITIES DEVELOPMENT COMMAND
CHEMICAL BIOLOGICAL CENTER